Valence tautomerism in synthetic models of cytochrome P450

Pradip Kumar Das[a,1], Subhra Samanta[a,1], Ashley B. McQuarters[b], Nicolai Lehnert[b,2], and Abhishek Dey[a,2]

[a]Department of Inorganic Chemistry, Indian Association for the Cultivation of Science, Kolkata 700032, India; and [b]Department of Chemistry, University of Michigan, Ann Arbor, MI 48109

Edited by Harry B. Gray, California Institute of Technology, Pasadena, CA, and approved May 2, 2016 (received for review January 16, 2016)

CytP450s have a cysteine-bound heme cofactor that, in its as-isolated resting (oxidized) form, can be conclusively described as a ferric thiolate species. Unlike the native enzyme, most synthetic thiolate-bound ferric porphyrins are unstable in air unless the axial thiolate ligand is sterically protected. Spectroscopic investigations on a series of synthetic mimics of cytP450 indicate that a thiolate-bound ferric porphyrin coexists in organic solutions at room temperature (RT) with a thiyl-radical bound ferrous porphyrin, i.e., its valence tautomer. The ferric thiolate state is favored by greater enthalpy and is air stable. The ferrous thiyl state is favored by entropy, populates at RT, and degrades in air. These ground states can be reversibly interchanged at RT by the addition or removal of water to the apolar medium. It is concluded that hydrogen bonding and local electrostatics protect the resting oxidized cytP450 active site from degradation in air by stabilizing the ferric thiolate ground state in contrast to its synthetic analogs.

valence tautomerism | cytochrome P450 | synthetic model | entropic contribution | hydrogen bonding

Heme bound to a cysteine ligand is found in the active sites of several key enzymes in biology, including cytochrome P450 (cytP450) and nitric oxide synthase (NOS), which broadly comprise the cytP450 superfamily (1, 2). Members of the cytP450 family of enzymes mediate key transformations in the synthesis of hormones and play an important role in the catabolism of metabolites and drugs (3). This subclass of heme enzymes distinguishes themselves by their ability to oxidize substrates using molecular O_2. The resting forms of their active sites are best described as an oxidized ferric heme bound to a thiolate ligand (the coordinating functional group of cysteine). The active sites in their resting ferric state are stable and only react with O_2 when they are reduced to the ferrous state (4, 5). This is in sharp contrast to the behavior of synthetic thiolate-bound ferric porphyrin complexes. Unless the thiolate is sterically protected, these synthetic ferric porphyrin complexes degrade in O_2 (6). This phenomenon has remained an enigma ever since the initial reports of synthetic thiolate-bound ferric porphyrin complexes by Holm and coworkers (7) and Collman and Sorrell (8) four decades ago. Similar sensitivity to O_2 by a formally oxidized metal center is exhibited by the active sites of ammine oxidase and intradiol dioxygenases (9, 10). The sensitivity to O_2 is significantly reduced in thiolate-bound ferric porphyrins in aqueous environments. In this case, recent work shows that heme–thiolate model systems can catalytically hydroxylate inert C–H bonds using molecular O_2 with >200 turnovers, i.e., bioinspired functional mimics of cytP450 (11). In addition, cytP450 enzymes form stable diamagnetic Fe^{III}–NO adducts (12). In contrast, attempts to form stable Fe^{III}–NO adducts of thiolate-bound iron porphyrin model systems inevitably results in the NO attacking the thiolate sulfur and not the iron. This is despite the fact that theoretical calculations predict these thiolate-bound porphyrin Fe^{III}–NO species to be stable entities (13). Curiously, similar sensitivity to O_2 is also exhibited by most nonheme ferric thiolate and many nickel thiolate complexes, which necessitates their handling in an inert atmosphere (14–16). This is particularly well established in the nonheme iron enzyme nitrile hydratase and its related synthetic models. Although the active site, when isolated in the absence of air, bears three cysteine thiolates and is inactive, its reaction with O_2 leads to the active form, which bears a cysteine sulfenate and a cysteine sulfinate as its ligands (17, 18). Similar transformations have been reproduced in synthetic model complexes (19).

The existing paradox of O_2 sensitivity of synthetic thiolate-bound ferric heme complexes thus requires an unusual electronic structure to be present in its genesis. Resonance Raman (rR), electron paramagnetic resonance (EPR), and ^{1}H NMR are useful tools to investigate the electronic structures of ferric heme complexes. In particular, the oxidation and spin state marker modes in the rR spectra of iron porphyrin complexes find abundant use in inorganic/bioinorganic spectroscopy (20). Synthetic iron porphyrin complexes show characteristic sets of ν_4 (1,340–1,375 cm^{-1}) and ν_2 (1,540–1,575 cm^{-1}) vibrations with very high fidelity (*SI Appendix*, Table S1). A series of iron porphyrin complexes with thiolate axial ligands (Fig. 1) are investigated here using a combination of rR, EPR, and ^{1}H NMR spectroscopy. These complexes are previously characterized and vary in the nature of the thiolate ligand; the aliphatic complex (Fig. 1*A*) is unstable in air and has an alkyl thiolate ligand (Fig. 1), the bulky aliphatic complex (Fig. 1*B*) has a sterically protected alkyl thiolate and is stable in air, the benzylic complex (Fig. 1*C*) is stable in air, and the aromatic thiolate (Fig. 1*D*) is unstable in air. Excitingly, the data presented here clearly suggest that these complexes exist as a mixture of two valence tautomers, namely, ferric thiolate and ferrous thiyl species, in the solid state and in solution.

Significance

Cytochrome P450 is a mammalian enzyme responsible for the catabolism of organic molecules (food, drug, etc.) as well as biosynthesis of hormones and cholesterol. Unfortunately, in stark contrast to the stability of the enzyme, its synthetic mimics rapidly degrade on being exposed to oxygen impeding erstwhile efforts of the scientific community to understand its chemistry in detail. Here the discovery of a valence tautomerism between a ferric thiolate and an arcane ferrous-thiyl species in synthetic models at room temperature is proposed to be at the root of this three-decade-old mystery. Hydrogen bonding to the thiolate sulfur, also present in the enzyme active site, restrains the system to the ferric thiolate form imparting its stability in the presence of oxygen.

Author contributions: N.L. and A.D. designed research; P.K.D., S.S., and A.B.M. performed research; S.S., N.L., and A.D. contributed new reagents/analytic tools; P.K.D., A.B.M., N.L., and A.D. analyzed data; and P.K.D., N.L., and A.D. wrote the paper.

The authors declare no conflict of interest.

This article is a PNAS Direct Submission.

[1]P.K.D. and S.S. contributed equally to this work.

[2]To whom correspondence may be addressed. Email: icad@iacs.res.in or lehnertn@umich.edu.

This article contains supporting information online at www.pnas.org/lookup/suppl/doi:10.1073/pnas.1600525113/-/DCSupplemental.

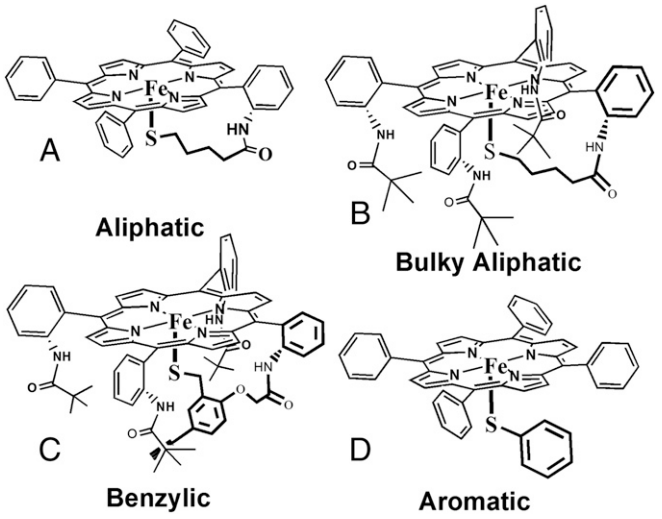

Fig. 1. Iron porphyrin complexes bearing axial thiolate ligands. (*A*) Aliphatic thiolate ligand, (*B*) aliphatic thiolate protected by bulky t-butyl groups, (*C*) benzyl thiolate, and (*D*) aromatic phenyl thiolate.

Results and Discussion

rR. rR data of the aliphatic complex (excitation wavelength, 413.1 nm) with axial alkyl-thiolate ligation show the ν_4 and ν_2 modes at 1,361 and 1,554 cm^{-1}, respectively, at 77 K [low temperature (LT)] in a weakly coordinating solvent like THF, indicating the presence of a high-spin Fe^{III} center (Fig. 2 *A* and *B*, blue dashed line). Similarly, the rR data of the aromatic complex shows the ν_4 and ν_2 vibrations at 1,361 and 1,553 cm^{-1} (Fig. 2*D*, blue dashed line). In a coordinating solvent such as MeOH, the ν_4 and ν_2 modes of the aliphatic-MeOH complex shift to 1,369 and 1,567 cm^{-1}, respectively, indicating the presence of a six-coordinate low-spin Fe^{III} center with methanol bound to the iron center (Fig. 2*A*, red dashed line). The rR data of the benzylic complex at LT in a weakly coordinating solvent like THF show the presence of ν_2 modes at 1,552 and 1,565 cm^{-1} originating from a high-spin and low-spin Fe^{III} species, respectively (Fig. 2*C*, blue dashed line). In MeOH solution, this complex shows only one set of ν_4 and ν_2 modes at 1,365 and 1,565 cm^{-1}, respectively, suggesting the presence of a low-spin Fe^{III} species in a coordinating solvent (Fig. 2*C*, red dashed line). Importantly, rR data of this series of thiolate-bound ferric porphyrin complexes, collected at room temperature (RT), show that there is a mixture of two species. One of them is the parent ferric thiolate species, and the other is characterized by the ν_4 and the ν_2 bands at 1,343–1,346 and 1,540–1,543 cm^{-1}, respectively (Fig. 2 *A–D*, blue solid line). Importantly, these values are characteristic of high-spin ferrous species. Although rR intensities are not quantitative, the relative intensities of the ferrous and ferric species at RT are comparable for all of these complexes. Furthermore, the change from a mixture of ferric and ferrous species at RT to a mostly ferric species at LT is completely reversible as the same mixture is obtained when the frozen solution is warmed up to RT and vice versa (*SI Appendix*, Fig. S1 *A–D*).

In the low-frequency region of the rR spectra, two vibrations are identified in the C–S region; one at 655 and one at 662 cm^{-1} (Fig. 3*A*, red and blue). At 77 K, only the 662 cm^{-1} vibration is observed, which shifts to 657 cm^{-1} on S^{34} substitution of the aromatic thiolate sulfur and to 647 cm^{-1} on deuterating the aromatic protons (Fig. 3*B*, blue to green; *SI Appendix*, Fig. S2) and represents the C–S stretching vibration of the PhS^- ligand bound to FeTPP. At RT, the 655 cm^{-1} vibration shifts to 653 cm^{-1} on S^{34} substitution and to 651 cm^{-1} on deuterating the aromatic

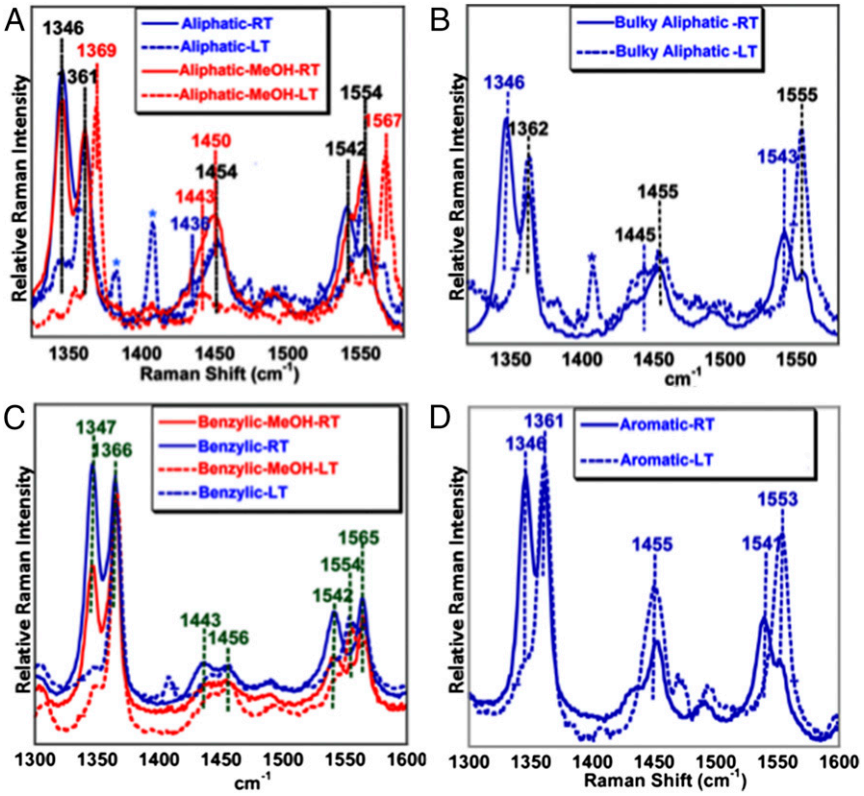

Fig. 2. rR data (413.1 nm, 10 mW) of the (*A*) aliphatic, (*B*) bulky aliphatic, (*C*) benzylic, and (*D*) aromatic complexes in THF (black) and MeOH (gray) at RT (bold line) and LT (dashed line). The asterisks (*) represent plasma lines from the laser.

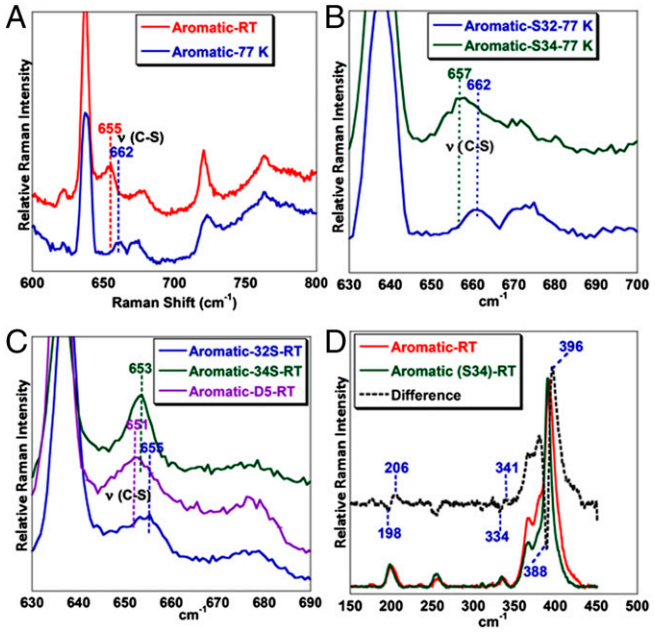

Fig. 3. rR data (413.1 nm, 5 mW) of (*A*) the aromatic complex at RT (red) and 77 K (blue), (*B*) ^{34}S isotopic substitution of aromatic complex at 77 K (green), (*C*) deuterated version of aromatic complex at RT (violet), and (*D*) difference spectrum in the Fe–S region of the aromatic complex in THF at RT (black).

protons (Fig. 3*C*, blue to green to violet) and represents the C–S stretching mode of the PhS· ligand bound to reduced Fe(II) porphyrin at RT (resonance enhancement by Soret not likely if not bound to the porphyrin). The Fe–S vibration for the Fe(III)–SR state is mixed with the ν_8 mode as evidenced by a 8 cm^{-1} shift in the ν_8 from 396 to 388 cm^{-1} on S^{34} substitution of the thiolate (Fig. 3*D*, red to green). The vibration at 341 cm^{-1} is a Fe(III)–SR stretching vibration and it shifts to 334 cm^{-1} on S^{34} substitution (Fig. 3*D*, red to green). Additionally, at RT, a vibration is observed at 206 cm^{-1} that shifts to 198 cm^{-1} on S^{34} substitution and could represent a Fe–S stretching mode (Fig. 3*D*, red to green). Thus, the 655 cm^{-1} and the 206 cm^{-1}, only observed at RT, and sensitive to S^{34} substitution may be assigned to the Fe–S and C–S vibration of the species at RT. The dramatic lowering of the Fe–S vibration in this species relative to the ferric thiolate species signifies substantial weakening of the Fe–S vibration from the Fe(III)–SR state to the Fe(II) species formed at RT.

EPR Spectroscopy. EPR data of the same series of thiolate-bound complexes at LT show that the iron centers in the complexes exist in its high-spin (S = 5/2) or low-spin (S = 1/2) ferric state in noncoordinating or coordinating solvents, respectively (Fig. 4). The iron center in the aliphatic complex is high spin in THF (Fig. 4, blue) and low spin in MeOH (Fig. 4, green). Thus, both the rR and EPR data collected at LT indicate that these thiolate-bound iron porphyrins can be described as ferric thiolate complexes consistent with previous reports. However, the rR data suggest that there is a significant decrease in the population of the ferric species and increase in population of a ferrous species in solution at RT relative to LT. The corresponding EPR data at RT show the increase in population of a radical species characterized by a signal at g = 2 (Fig. 4, red) relative to the data obtained at LT. Although, expectedly, the EPR data at RT do not show significant intensity of the g = 6 signal from the high-spin ferric species present in solution, the solution rR data under the same conditions clearly demonstrate the presence of both ferric and ferrous porphyrin species. These data suggest that, apart from the ferric thiolate species, a ferrous ligand radical species exists at RT. Note that the ferrous ligand radical species is a valence tautomer of the ferric thiolate complex. Spin quantification of this radical signal at RT indicates that the population of this species for the aliphatic, bulky aliphatic, benzylic, and aromatic thiolate complexes are 52%, 50%, 46%, and 45%, respectively.

NMR Spectroscopy. ^{1}H NMR is routinely used as a probe for the oxidation and spin state of ferric porphyrin complexes. The β-pyrrole resonances are shifted between 60 and 80 ppm for high-spin ferrous and ferric porphyrin complexes at 298 K (21). The imidazole-bound iron porphyrin complex (PIM) shows one broad β-pyrrole resonance at 80 ppm (*SI Appendix*, Fig. S3), as expected for a high-spin ferric porphyrin at 289 K. On the contrary, all of the thiolate-bound porphyrins show two sets of resonances at 298 K in the 40- to 80-ppm region, which might correspond to the individual signals of the high-spin ferrous and ferric porphyrin complexes in solution. This, however, would require that the switch between the two ground states would be slow enough at RT to be resolved on the NMR timescale, and it is not clear at this point whether this requirement is fulfilled. For example, the data for the aliphatic complex, obtained at 273 K, show the Fe^{III} pyrrole resonances at 85 ppm (*SI Appendix*, Fig. S3). There is a resonance at ∼45 ppm characteristic of a high-spin ferrous porphyrin, consistent with the rR data, but these resonances may be effected by the resonances of the ligand radical present. On the other hand, for the aromatic complex, the signal at 57–60 ppm at RT is consistent with previous reports (22).

Variable-Temperature and Radical Trapping Experiments. The conversion of the mixture of ferrous and ferric porphyrins at RT to the ferric porphyrin at LT is continuous as reflected in the variable temperature (VT) rR data. The VT rR data of the aliphatic complex in THF show that the ν_4 and ν_2 bands at 1,344 and 1,536 cm^{-1}, corresponding to the high-spin ferrous porphyrin, lose intensity as the temperature is gradually lowered and those for the high-spin ferric species (1,361 and 1,554 cm^{-1}) increase (*SI Appendix*, Fig. S4, *Left*). Similarly, the ν_2 and the ν_4 bands of the benzylic and aromatic complexes corresponding to the high-spin ferrous component lose intensity with decreasing temperature and those of the ferric porphyrin gain intensity (Fig. 5). This appearance of the radical signal at RT and its reversibility is further indicated from VT EPR data (*SI Appendix*, Fig. S4, *Right*). The radical signal at g = 2.05–2.03 observed at RT reduces in intensity as the temperature is gradually

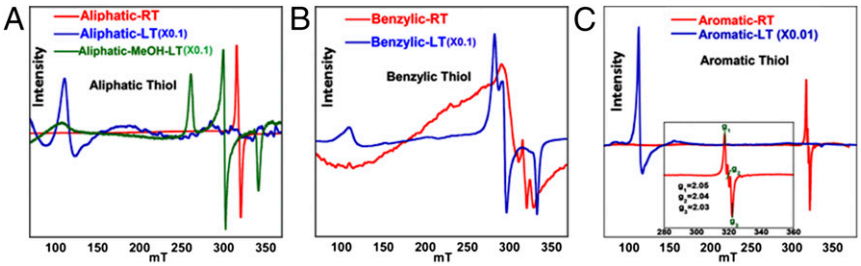

Fig. 4. EPR data of the (*A*) aliphatic, (*B*) benzylic, and (*C*) aromatic complexes in toluene at RT (red) and LT (blue). Note that the LT spectrum in *C* is measured at 10 K.

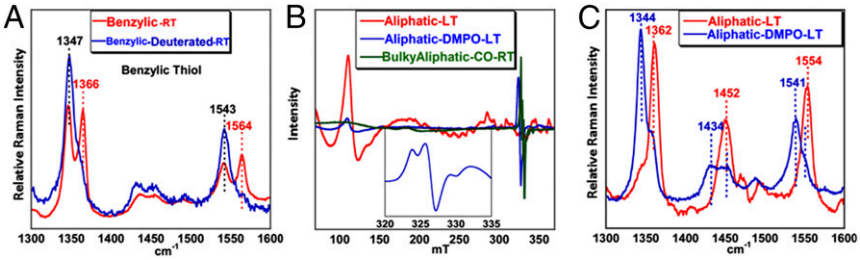

Fig. 5. (*A*) rR data of the benzylic thiolate (red) and the deuterated benzyl thiolate (blue) at RT in THF. (*B*) EPR spectra of the DMPO adduct of the aliphatic thiolate (blue) and CO-bound bulky aliphatic complex (green) in toluene at RT and (*C*) rR data (413.1 nm, 10 mW) of the aliphatic complex (red) and aliphatic plus DMPO (blue) in THF.

reduced. The radical signal regains intensity when the temperature of the sample is gradually increased to RT. Similar transitions between ferric and radical signals are observed for the benzylic and aromatic thiolate-bound complexes as well (*SI Appendix*, Figs. S6 and S7). VT absorption data on the aliphatic thiolate-bound complexes is obtained in THF solution. The data indicate that transitions at 320, 419, 522, and 670 nm gain intensity as the temperature is lowered with isosbestic points at 330 and 600 nm (*SI Appendix*, Fig. S8). Analyses of these data indicate that the ferric thiolate state for the aliphatic complex is favored by ΔH of 5.6 kcal/mol, whereas the ferrous-thiyl state is favored by ΔS of 21.8 cal·mol^{-1}·K^{-1}.

The spectroscopic data are consistent with the presence of valence tautomerism in thiolate-bound iron porphyrin model complexes, irrespective of the nature of the thiolate ligand. The possibility of a $Fe^{III} + RS^- = Fe^{II} + RSSR$ process is eliminated by the fact that these changes are reversible with temperature and the resultant disulfide species [free thiyl radical has $t_{1/2} < 10^{-9}$ s (23)] is diamagnetic and, hence, would not give rise to the significant population of the radical at RT. Furthermore, when ethane thiol is added to a solution of Fe^{III} porphyrin, the resultant solution shows Fe^{II} porphyrin (*SI Appendix*, Fig. S9) irrespective of the temperature, further indicating that a $Fe^{III} + RS^- = Fe^{II} + RSSR$ equilibrium is not responsible for the reversible conversion between the Fe^{III} and Fe^{II} states observed here. Porphyrin cation radicals are characterized by very weak bands in the rR spectrum, with ν_4 and ν_2 vibrations at 1,351 and 1,532 cm^{-1}, respectively. These are not consistent with our data, which show clear rR signatures of high-spin ferrous porphyrins for the additional species observed at RT. This raises the possibility of a Fe^{III}–RS^- ↔ Fe^{II}–RS· valence tautomerism in these complexes. This would require the radical species, observed at RT, to be a thiyl radical. The g values of this radical signal observed at room temperature in solution range from 2.05 to 2.03 typical for metal-bound thiyl radicals in solution (24, 25). Furthermore, on incubation of the aliphatic complex with 5,5-dimethyl-1-pyrroline-*N*-oxide (DMPO), the EPR data show a dominate radical signal, even at LT, indicating the formation of a thiyl adduct of DMPO, and only a very weak signal corresponding to Fe^{III} is detected (Fig. 5*B*, blue). The corresponding rR data of this species show the ν_4 and ν_2 vibrations at 1,344 and 1,541 cm^{-1}, suggesting the presence of a high-spin Fe(II) center in this complex (Fig. 5*C*, blue). One might expect the spin on the thiyl radical to couple with the S = 2 Fe^{II} center. It is possible that either the relaxation of the signal arising from the Fe^{II} center is too fast at RT to be detected in EPR or the coupling between the metal spin and the ligand spin is too weak as has been reported in some transition metal complexes (26–28). Although density functional theory (DFT) calculation cannot provide optimized geometry of species with higher entropy, a potential energy scan of the Fe–S bond of the aliphatic thiol complex indicates (*SI Appendix*, Fig. S10) that the spin density on the thiolate sulfur increases above 0.5, implying increase in thiyl character, when the Fe–S bond is 2.5 Å, i.e., ~0.2 Å longer than the DFT-calculated equilibrium Fe–S distance of the ferric thiolate state. Note that the proposed weak Fe–S vibration at 206 cm^{-1} observed at RT is consistent with the formation of a Fe^{II}-thiyl species.

To confirm that the radical is indeed a thiyl radical, a deuterated version of the benzylic complex was prepared where the benzylic and the aromatic protons are replaced with deuterium. A vibration at 1,260 cm^{-1} is observed to shift to 914 cm^{-1} upon deuteration of the thiolate ligand. This mode, which is only observed at RT and is thus unique to the radical state, represents a benzylic CH_2 wagging mode, coupled to the C–S stretch. The observed H/D isotope shift is consistent with that predicted by DFT calculations on a benzyl thiyl radical (*SI Appendix*, Fig. S11). The rR data of this complex show that it exists almost exclusively as a ferrous species at RT and reversibly converts to a ferric species at low temperatures (Fig. 5*A*, red to blue). The entropic contribution leading to the change of ground state at RT thus seems to be derived from the population of low-lying C–H vibrational modes of the thiolate ligand in the ferrous thiyl state. The substitution of these C–H units by C–D lowers the energy of these modes, increasing their populations and leading to a greater entropic stabilization of the ferrous thiyl radical state at RT. A similar gain in entropy is proposed to stabilize the entatic state of blue Cu proteins with axial methionine ligands, which results in low-frequency vibrational and rotational modes involving the methyl and methylene side chains of the methionine (29). Our data provide direct evidence for the presence of Fe^{III}–RS^- ↔ Fe^{II}–RS· valence tautomerism in these model complexes similar to those reported for some metal dithiolenes.

The conversion of Fe^{II}-thiyl to Fe^{III}-thiolate at low temperatures could be arrested when CO is added to a solution of the bulky aliphatic complex in THF at RT. A sharp Soret band at 418 nm and a Q band at 538 nm are observed, suggesting the formation of a Fe–CO species which dominates the absorption spectrum (*SI Appendix*, Fig. S12*A*). These features are quite different from the ferrous CO complex, which features a Soret band at 445 nm and a Q band at 567 nm (30). The rR data of this CO adduct show a major species with ν_4 and ν_2 bands at 1,366 and 1,564 cm^{-1} and two new bands at 522 and 1,953 cm^{-1} (*SI Appendix*, Fig. S12 *B–D*). A minor high-spin ferric species with a ν_2 at 1,555 cm^{-1} is also present. The EPR data of this complex show a sharp radical signal at RT with a g value of 2.04 consistent with a thiyl radical (Fig. 5*B*, gray). Spin quantification of this signal against TEMPO indicates 78 ± 3% population at RT.

Note that the EPR data of these complexes in the solid state show the presence of the same radical signal at RT as well as at LT (*SI Appendix*, Fig. S13). The inability of these complexes to exhibit reversible temperature-dependent valence tautomerism in the solid state implies that the process entails a change in geometry of these complexes that is only possible in solution.

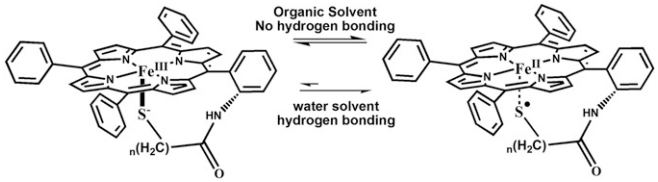

Fig. 6. Schematic representation of the valence tautomerism equilibrium.

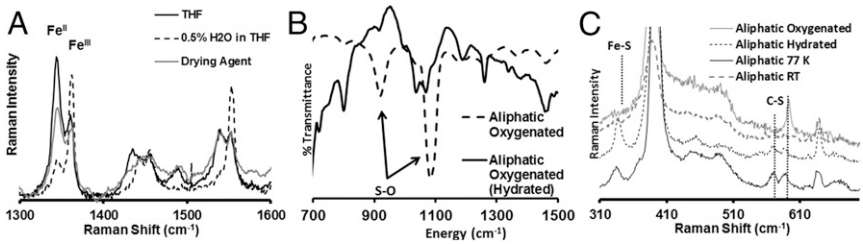

Fig. 7. rR data of the air stable (*A*) bulky aliphatic complex in THF (black) and in the presence of 0.5% H_2O (dashed line) and after dehydration with activated $MgSO_4$ (gray), (*B*) IR data of the aliphatic complex, and (*C*) rR data of the aliphatic complex in oxygenated THF (gray) and in 0.5% H_2O/THF (small dashes) at RT as well as at LT (black).

Thermal population of an excited state does not require a change in geometry and would occur in the solid state as well. Similarly, spin quantification of the radical signal at RT indicated more than 50% population at RT. Thus, it seems most likely that the valence tautomers are in equilibrium with each other in solution (change in ground state, Fig. 6). Using the ΔH and ΔS values, obtained from the VT observation data, the K_{eq} at RT is estimated to be 4.57, 4.30, and 4.20 for the aliphatic, benzylic, and aromatic thiolate complexes, respectively, in THF.

The Role of Hydrogen Bonds. rR data of the bulky aliphatic and benzylic complexes when attached to self-assembled monolayers of thiols on Ag surfaces (*SI Appendix*, Fig. S14 *A* and *B*, blue) and dipped in aqueous solution show the presence of only ferric thiolate species (30, 31). In contrast to the data observed in organic solution (*SI Appendix*, Fig. S14 *A* and *B*, red), the ν_4 and ν_2 modes at 1,343 and 1,542 cm^{-1} corresponding to ferrous species are not observed in these cases. The equilibrium of ferrous thiyl and ferric thiolate species in solution is completely shifted to a ferric thiolate state when hydrated with only 0.5% H_2O (by volume) in THF at RT (Fig. 7*A*, black to dashed line). The equilibrium could be reinstated (Fig. 7*A*, black to gray) by dehydrating the THF solution using a moisture adsorbent ($MgSO_4$). Thus, the aqueous environment stabilizes the ferric thiolate state only. In these heterogeneous systems, the thermodynamic reduction potentials (E^0 $Fe^{III/II} = 0.0$ V vs. NHE) are shifted toward positive potentials relative to analogous synthetic complexes in organic medium (–0.3 V vs. NHE) consistent with the presence of hydrogen bonding to the axial thiolate ligand (32, 33). We propose that similar hydrogen bonding interaction of the thiolate ligand with water shifts the equilibrium to the Fe^{III}–thiolate state. The conversion to the ferric thiolate state indeed imparts tolerance to O_2 in these systems as indicated by the fact that, although the aliphatic thiolate complex readily degrades in O_2 in THF resulting in sulfur oxidation (S–O vibration at 1,080 and 918 cm^{-1}; Fig. 7*B*, dashed line), this complex is quite stable in the presence of 0.5% H_2O (Fig. 7*B*, black line). In parallel, the Fe–S and C–S vibrations in the rR spectrum of this complex dissolved in THF are lost when exposed to O_2 but retained in the presence of 0.5% H_2O (Fig. 7*C*).

Conclusions

In summary, rR, H^1 NMR, and EPR data, collected at LT, indicate that thiolate-bound model complexes are best described as high-spin ferric porphyrins, consistent with previous literature reports. Synthetic models fit the description of the cytP450 active site. However, the VT, rR, H^1 NMR, and EPR data show the presence of a temperature-dependent valence tautomerism between the ferric thiolate and a ferrous thiyl species, with significant amounts of ferrous thiyl species present in solution at RT. The thiyl radical of the latter species could be trapped as a DMPO adduct, and formation of this species was further driven by CO coordination to the heme. The presence of the ferrous-thiyl state helps explain the mysteriously high sensitivity of synthetic thiolate-bound ferric porphyrin mimics of cytP450 toward O_2, which is not exhibited by ferric porphyrins having any other innocent axial ligand, as well as their instability toward a free radical like nitric oxide. O_2 sensitivity exhibited by thiolate bound nonheme iron systems (e.g., Nitrile hydratase) and in synthetic complexes may have very similar origins. This situation is comparable to O_2 activation by the cupric active site of ammine oxidase and the ferric site of intradiol dioxygenase, where a valence tautomer of the resting oxidized state involving an oxidized ligand radical and the reduced metal center is heralded as the active form (34, 35). The enzyme active sites bearing cysteine-bound hemes, on the contrary, are established to exist in their ferric thiolate forms and hence are stable in O_2. Although the protein active sites of these enzymes are hydrophobic, quite like the organic solvents used here, there is at least one hydrogen-bonding interaction present between the protein backbones to the cysteine thiolate sulfur (Fig. 8, *Left*, dashed line) (36–38). In the past, much research has been devoted toward understanding the function and significance of these hydrogen bonds for P450 catalysis (39–41). Overlay of structures of several members of the cytP450 family shows that the secondary structure near the cysteine ligand is quite conserved (Fig. 8, *Right*, GXCY where X and Y are hydrophobic residues). The stereochemistry of this loop is as such that three amide dipoles present in this loop are pointed toward the cysteine S (the NH amide between GX corresponds to the conserved hydrogen bond to the cysteine). This results in a positive electrostatic potential near the cysteine sulfur (Fig. 8, *Right*). It is conceivable that the hydrogen bond and the peptide electrostatics stabilize the ferric thiolate state relative to the ferrous thiyl state due to the presence of higher charge separation in the former (42). Accordingly, we have observed that thiolate-bound iron porphyrin complexes dissolved in organic solvent containing 0.5% water and when immobilized on the surface of electrodes in an aqueous environment show the presence of a dominant ferric thiolate ground state at RT. It is possible that hydrogen bonding in these systems mimic those present in the protein active sites resulting in the stabilization of the ferric thiolate state in an aqueous environment in contrast to exhibiting the ferric thiolate and ferrous thiyl radical equilibrium in nonpolar organic solvents, which are devoid of any hydrogen-bonding interactions. In systems where the thiolate sulfur is sterically protected (e.g., the bulky aliphatic thiolate complex), the ferrous center generates O_2^-, which degrades the porphyrin macrocycle (*SI Appendix*, Fig. S15). Our results, therefore, indicate that one of the most important functions of the hydrogen bond to the cysteine ligand could be the stabilization of the ferric-thiolate ground state

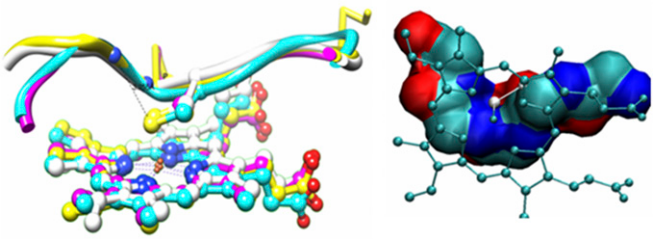

Fig. 8. (*Left*) The conserved secondary structure near the coordinated cysteine and (*Right*) the resulting electrostatic potential experienced by the cysteine sulfur.

of the heme, to prevent catastrophic degradation of the CytP450 active site in its (oxidized) resting state by O_2.

Materials and Methods

The organic solvents used are purified by distilling them in the presence of the appropriate drying agent. The solvents were degassed by three to five freeze–pump–thaw cycles and stored in an MBraun N_2 glove box to prepare the solutions. All reactions were performed under inert conditions using Schlenk techniques. The aliphatic, bulky aliphatic, and benzylic complexes were synthesized as previously described in refs. 30 and 43. The details of the data obtained under heterogeneous conditions are provided in refs. 31 and 44. The synthesis of the [Fe(TPP)(SPh)] (aromatic) complex was carried out using solvents that were dried over CaH_2 and distilled under argon. The purified solvents were degassed via six freeze–pump–thaw cycles and stored in an MBraun glove box equipped with a circulating purifier (O_2, H_2O < 0.1 ppm). The resonance Raman experiments were performed using a Coherent Sabre Kr ion laser and a Princeton Instruments Trivista 555 triple monochromator spectrograph fitted with a Pixis Excelion CCD camera for all complexes. The EPR data were collected on a Jeol instrument at the IACS EPR facility. The ^1H NMR spectra were obtained on a Bruker DPX-300 or a DPX-500 instrument at RT (25 °C) as well as LT (–60 °C) in $CDCl_3$ solvent. The absorption data were collected on an Agilent Technology 8453 spectrophotometer.

The resonance Raman data were collected using 413.1-nm laser excitation by irradiating the sample with <10-mW power. Normally, the data are collected using a 45° backscattering configuration. The stray light is rejected using the first two stages of the Trivista monochromator as a tunable band pass. The VT data are collected using a home-built setup where the temperature of a sample is maintained by controlling the flow of He gas cooled by passing it through a Cu tube immersed in liquid N_2. The temperature is adjusted by controlling the flow of the cold N_2 gas and measured in situ using an alcohol thermometer. The typical sample concentration is 1 mM. It is very important to avoid air leaking into the sample tubes during these experiments. Spin quantification (double integration of the EPR signal) of the samples were carried out at RT against a 1 mM solution of (2,2,6,6-tetramethylpiperidin-1-yl)oxyl or (2,2,6,6-tetramethylpiperidin-1-yl)oxidanyl (TEMPO). The TEMPO solution in turn was calibrated against a 1 mM solution of Cu^{2+} standard solution (1 mM $CuSO_4$ in 1 N $HClO_4$) at 77 K. The spin quantification of the CO complexes was carried out against 1 mM Cu^{2+} standard solution at 77 K.

ACKNOWLEDGMENTS. We acknowledge Prof. Harry B. Gray (California Institute of Technology) for his insightful comments and suggestions on the manuscript. This research was funded by SB/S1/IC-25/2013 (to A.D.); Department of Science and Technology, Government of India; and National Science Foundation Grant CHE-1464696 (to N.L.).

1. Denisov IG, Makris TM, Sligar SG, Schlichting I (2005) Structure and chemistry of cytochrome P450. *Chem Rev* 105(6):2253–2277.
2. Sono M, Roach MP, Coulter ED, Dawson JH (1996) Heme-containing oxygenases. *Chem Rev* 96(7):2841–2888.
3. Whitehouse CJC, Bell SG, Wong L-L (2012) P450(BM3) (CYP102A1): Connecting the dots. *Chem Soc Rev* 41(3):1218–1260.
4. Dawson JH, Sono M (1987) Cytochrome P-450 and chloroperoxidase: Thiolate-ligated heme enzymes. Spectroscopic determination of their active-site structures and mechanistic implications of thiolate ligation. *Chem Rev* 87(5):1255–1276.
5. Meunier B, de Visser SP, Shaik S (2004) Mechanism of oxidation reactions catalyzed by cytochrome p450 enzymes. *Chem Rev* 104(9):3947–3980.
6. Higuchi T, Uzu S, Hirobe M (1990) Synthesis of a highly stable iron porphyrin coordinated by alkylthiolate anion as a model for cytochrome P-450 and its catalytic activity in oxygen-oxygen bond cleavage. *J Am Chem Soc* 112(19):7051–7053.
7. Koch S, Tang SC, Holm RH, Frankel RH, Ibers JA (1975) Letter: Ferric porphyrin thiolates. Possible relationship to cytochrome P-450 enzymes and the structure of (*p*-nitrobenzenethiolato)iron(III) protoporphyrin IX dimethyl ester. *J Am Chem Soc* 97(4):916–918.
8. Collman JP, Sorrell TN (1975) Letter: A model for the carbonyl adduct of ferrous cytochrome P450. *J Am Chem Soc* 97(14):4133–4134.
9. Ghosh S, et al. (2008) Spectroscopic and electronic structure studies of phenolate Cu(II) complexes: Phenolate ring orientation and activation related to cofactor biogenesis. *J Am Chem Soc* 130(48):16262–16273.
10. Pau MYM, Lipscomb JD, Solomon EI (2007) Substrate activation for O_2 reactions by oxidized metal centers in biology. *Proc Natl Acad Sci USA* 104(47):18355–18362.
11. Sengupta K, Chatterjee S, Samanta S, Bandyopadhyay S, Dey A (2013) Resonance Raman and electrocatalytic behavior of thiolate and imidazole bound iron porphyrin complexes on self assembled monolayers: Functional modeling of cytochrome P450. *Inorg Chem* 52(4):2000–2014.
12. Yang H, Gandhi H, Ostrom NE, Hegg EL (2014) Isotopic fractionation by a fungal P450 nitric oxide reductase during the production of N_2O. *Environ Sci Technol* 48(18):10707–10715.
13. Hunt AP, Lehnert N (2015) Heme-nitrosyls: Electronic structure implications for function in biology. *Acc Chem Res* 48(7):2117–2125.
14. Kovacs JA, Brines LM (2007) Understanding how the thiolate sulfur contributes to the function of the non-heme iron enzyme superoxide reductase. *Acc Chem Res* 40(7):501–509.
15. Chohan BS, Shoner SC, Kovacs JA, Maroney MJ (2004) Ligand oxidations in high-spin nickel thiolate complexes and zinc analogues. *Inorg Chem* 43(24):7726–7734.
16. Grapperhaus CA, Darensbourg MY (1998) Oxygen capture by sulfur in nickel thiolates. *Acc Chem Res* 31(8):451–459.
17. Dey A, et al. (2006) Sulfur K-edge XAS and DFT calculations on nitrile hydratase: Geometric and electronic structure of the non-heme iron active site. *J Am Chem Soc* 128(2):533–541.
18. Noguchi T, Nojiri M, Takei K, Odaka M, Kamiya N (2003) Protonation structures of Cys-sulfinic and Cys-sulfenic acids in the photosensitive nitrile hydratase revealed by Fourier transform infrared spectroscopy. *Biochemistry* 42(40):11642–11650.
19. Kovacs JA (2004) Synthetic analogues of cysteinate-ligated non-heme iron and non-corrinoid cobalt enzymes. *Chem Rev* 104(2):825–848.
20. Burke JM, et al. (1978) Structure-sensitive resonance Raman bands of tetraphenyl and "picket fence" porphyrin-iron complexes, including an oxyhemoglobin analog. *J Am Chem Soc* 100(19):6083–6088.
21. Walker FA (1999) Magnetic spectroscopic (EPR, ESEEM, Mossbauer, MCD and NMR) studies of low-spin ferriheme centers and their corresponding heme proteins. *Coord Chem Rev* 185-186(0):471–534.
22. Arasasingham RD, et al. (1990) Proton NMR studies of iron(III) porphyrins with axial phenoxide or thiophenoxide ligands. *Inorg Chem* 29(10):1847–1850.
23. Tripathi GNR, Sun Q, Armstrong DA, Chipman DM, Schuler RH (1992) Resonance Raman spectra and structure of phenylthiyl radical. *J Phys Chem* 96(13):5344–5350.
24. Sievers C, Deters D, Hartmann H-J, Weser U (1996) Stable thiyl radicals in dried yeast Cu(I)6-thionein. *J Inorg Biochem* 62(3):199–205.
25. Kimura S, Bill E, Bothe E, Weyhermüller T, Wieghardt K (2001) Phenylthiyl radical complexes of gallium(III), iron(III), and cobalt(III) and comparison with their phenoxyl analogues. *J Am Chem Soc* 123(25):6025–6039.
26. Verma P, Pratt RC, Storr T, Wasinger EC, Stack TDP (2011) Sulfanyl stabilization of copper-bonded phenoxyls in model complexes and galactose oxidase. *Proc Natl Acad Sci USA* 108(46):18600–18605.
27. Buchanan RM, Pierpont CG (1980) Tautomeric catecholate-semiquinone interconversion via metal-ligand electron transfer. Structural, spectral, and magnetic properties of (3,5-di-tert-butylcatecholato)(3,5-di-tert-butylsemiquinone)(bipyridyl)cobalt(III), a complex containing mixed-valence organic ligands. *J Am Chem Soc* 102(15):4951–4957.
28. Konarev DV, et al. (2015) Synthesis, structures, and properties of crystalline salts with radical anions of metal-containing and metal-free phthalocyanines. *Chemistry* 21(3):1014–1028.
29. Ghosh S, et al. (2009) Thermodynamic equilibrium between blue and green copper sites and the role of the protein in controlling function. *Proc Natl Acad Sci USA* 106(13):4969–4974.
30. Samanta S, et al. (2013) O_2 reduction reaction by biologically relevant anionic ligand bound iron porphyrin complexes. *Inorg Chem* 52(22):12963–12971.
31. Chatterjee S, Sengupta K, Samanta S, Das PK, Dey A (2015) Concerted proton-electron transfer in electrocatalytic O_2 reduction by iron porphyrin complexes: Axial ligands tuning H/D isotope effect. *Inorg Chem* 54(5):2383–2392.
32. Dey A, et al. (2007) Sulfur K-edge X-ray absorption spectroscopy and density functional theory calculations on superoxide reductase: Role of the axial thiolate in reactivity. *J Am Chem Soc* 129(41):12418–12431.
33. Dey A, et al. (2005) Sulfur K-edge XAS and DFT calculations on P450 model complexes: Effects of hydrogen bonding on electronic structure and redox potentials. *J Am Chem Soc* 127(34):12046–12053.
34. Janes SM, et al. (1990) A new redox cofactor in eukaryotic enzymes: 6-Hydroxydopa at the active site of bovine serum amine oxidase. *Science* 248(4958):981–987.
35. Costas M, Mehn MP, Jensen MP, Que L, Jr (2004) Dioxygen activation at mononuclear nonheme iron active sites: Enzymes, models, and intermediates. *Chem Rev* 104(2):939–986.
36. Yano JK, Hsu M-H, Griffin KJ, Stout CD, Johnson EF (2005) Structures of human microsomal cytochrome P450 2A6 complexed with coumarin and methoxsalen. *Nat Struct Mol Biol* 12(9):822–823.
37. Sligar SG (2010) Chemistry. Glimpsing the critical intermediate in cytochrome P450 oxidations. *Science* 330(6006):924–925.
38. Raag R, Martinis SA, Sligar SG, Poulos TL (1991) Crystal structure of the cytochrome P-450CAM active site mutant Thr252Ala. *Biochemistry* 30(48):11420–11429.
39. de Visser SP, Ogliaro F, Sharma PK, Shaik S (2002) Hydrogen bonding modulates the selectivity of enzymatic oxidation by P450: Chameleon oxidant behavior by compound I. *Angew Chem Int Ed Engl* 41(11):1947–1951.
40. Galinato MGI, Spolitak T, Ballou DP, Lehnert N (2011) Elucidating the role of the proximal cysteine hydrogen-bonding network in ferric cytochrome P450cam and corresponding mutants using magnetic circular dichroism spectroscopy. *Biochemistry* 50(6):1053–1069.
41. Roach MP, Pond AE, Thomas MR, Boxer SG, Dawson JH (1999) The role of the distal and proximal protein environments in controlling the ferric spin state and in stabilizing thiolate ligation in heme systems: Thiolate adducts of the myoglobin H93G cavity mutant. *J Am Chem Soc* 121(51):12088–12093.
42. Ogliaro F, Cohen S, de Visser SP, Shaik S (2000) Medium polarization and hydrogen bonding effects on compound I of cytochrome P450: What kind of a radical is it really? *J Am Chem Soc* 122(51):12892–12893.
43. Das PK, Chatterjee S, Samanta S, Dey A (2012) EPR, resonance Raman, and DFT calculations on thiolate- and imidazole-bound iron(III) porphyrin complexes: role of the axial ligand in tuning the electronic structure. *Inorg Chem* 51(20):10704–10714.
44. Chatterjee S, Sengupta K, Samanta S, Das PK, Dey A (2013) Electrocatalytic O_2 reduction reaction by synthetic analogues of cytochrome P450 and myoglobin: in-situ resonance Raman and dynamic electrochemistry investigations. *Inorg Chem* 52(17):9897–9907.